THE ASTROPHYSICAL JOURNAL, 541:1033–1050, 2000 October 1

CORE-COLLAPSE SIMULATIONS OF ROTATING STARS

CHRIS L. FRYER AND ALEXANDER HEGER
Lick Observatory, University of California Observatories, Santa Cruz, CA 95064; cfryer@ucolick.org, alex@ucolick.org
Received 1999 June 21; accepted 2000 May 4

ABSTRACT

We present the results from a series of two-dimensional core-collapse simulations using a rotating progenitor star. We find that the convection in these simulations is less vigorous because (1) rotation weakens the core bounce that seeds the neutrino-driven convection and (2) the angular momentum profile in the rotating core stabilizes against convection. The limited convection leads to explosions that occur later and are weaker than the explosions produced from the collapse of nonrotating cores. However, because the convection is constrained to the polar regions, when the explosion occurs it is stronger along the polar axis. This asymmetric explosion may explain the polarization measurements of core-collapse supernovae. These asymmetries also provide a natural mechanism to mix the products of nucleosynthesis out into the helium and hydrogen layers of the star. We also discuss the role the collapse of these rotating stars plays in the generation of magnetic fields and neutron star kicks. Given a range of progenitor rotation periods, we predict a range of supernova energies for the same progenitor mass. The critical mass for black hole formation also depends upon the rotation speed of the progenitor.

Subject headings: black hole physics — convection — hydrodynamics — stars: interiors — stars: rotation — supernovae: general

1. INTRODUCTION

The study of the collapse of *rotating* massive stars is nearly as old as the study of core-collapse supernovae themselves. Four years after the first numerical simulations of neutrino-powered core-collapse supernovae (Colgate & White 1966), LeBlanc & Wilson (1970) modeled the core collapse of a rotating massive star. LeBlanc & Wilson (1970) proposed that, instead of using neutrinos to convert gravitational energy into kinetic energy and to power the explosion (Colgate & White 1966), supernovae were powered by the conversion of rotational energy using magnetic fields. Although neutrino heating is now considered to be the dominant power source driving supernovae, the importance of rotation remains a matter of dispute.

Most of the recent work studying the collapse of rotating massive stars has concentrated on the emission of gravitational waves (Müller, Różyczka, & Hillebrandt 1980; Tohline, Schombert, & Boss 1980; Finn & Evans 1990; Mönchmeyer et al. 1991; Bonazzola & Marck 1993; Yamada & Sato 1995; Zwerger & Müller 1997; Rampp, Müller, & Ruffert 1998). Some of the work, however, was devoted to understanding the effect of rotation upon the supernova explosion itself (Müller & Hillebrandt 1981; Bodenheimer & Woosley 1983; Symbalisty 1984; Mönchmeyer & Müller 1989; Janka & Mönchmeyer 1989; Janka, Zwerger, & Mönchmeyer 1993; Yamada & Sato 1994). Currently, no consensus on the effects of rotation has been reached. For instance, there is still disagreement on whether rotation increases or decreases the explosion energy. Mönchmeyer & Müller (1989) found that, in most cases, rotation weakens the core bounce, which ultimately weakens the explosion. On the other hand, the asymmetry in the neutrino emission caused by rotation may help seed convection, increasing the efficiency of neutrino heating and ultimately producing a more powerful explosion (Yamada & Sato 1994).

The simplifying assumptions in all of these simulations make it difficult to resolve this disagreement. For instance, none of the above simulations incorporated neutrino transport into their multidimensional hydrodynamic simulations. Many of the simulations use extremely simplified equations of state, which, as Müller & Hillebrandt (1981) discovered, alters significantly the effect of rotation. In addition, the precollapse cores used in the supernova models were all created assuming no rotation,[1] and the angular momentum was then added artificially prior to the collapse simulation.

Two major advances in supernova theory seek to resolve the question of rotation effects on core collapse. First, in the past five years, codes have been developed with the necessary equations of state and neutrino physics to model the core collapse in two dimensions from the initial collapse all the way through explosion (Herant et al. 1994; Burrows, Hayes, & Fryxell 1995; Fryer 1999). In addition to improvements on the collapse codes, Heger (1998) and Heger, Langer, & Woosley (2000) have evolved rotating massive stars to core collapse using a prescription for the transport of angular momentum, producing rotating core-collapse progenitors. In this paper, we present results of collapse simulations of these rotating massive cores.

In § 2 we outline the assumptions of the progenitor models and discuss the specific progenitor we use in our simulations. The core collapse code is described in § 3, and the basic effects of rotation are outlined in § 4. We find that not only is the bounce of our rotating stars weaker, but the angular momentum in the star stabilizes the core, constraining convection to the poles. These two effects decrease dramatically the efficiency at which convection is able to convert neutrino energy into kinetic energy. The net effect is to delay the supernova explosion, producing larger compact remnants and weaker explosions. We present the explosion simulations for all our models in § 5. The asymmetry in the convection produces asymmetric explosions that may explain polarization measurements of supernovae and may inject α-elements deep into the star's envelope. We

[1] Zwerger & Müller (1997) used rotating equilibrium polytropes to study gravitational wave emission.

conclude by reviewing the implications of these results for core-collapse supernovae, black hole formation, and the collapsar model for gamma-ray bursts.

2. PROGENITOR

All of the previous collapse simulations of rotating cores prescribed an angular momentum profile onto a nonrotating progenitor. For our simulations, we use the 15 $M_{\odot}$ rotating progenitor E15B of Heger et al. (2000). At central hydrogen ignition, this model has a "solar" composition (Grevese & Noels 1993) and an equatorial rotation velocity of 200 km s^{-1}, which is a typical value for these stars (e.g., Fukuda 1982). The transport of angular momentum and chemical mixing were modeled using a technique similar to that of Endal & Sophia (1978), and the parameterization used for the different mixing efficiencies was similar to that of Pinsonneault et al. (1989). The rotationally induced mixing processes include dynamical and secular shear instability, Solberg-Høiland instability, Goldreich-Schubert-Fricke instability, and Eddington-Sweet circulation. All these mixing processes, as well as the convective instability, were assumed to lead to rigid rotation on their corresponding timescale (Fig. 1 shows the evolution of the angular momentum at various stages of the star's life). Equipotential surfaces were assumed to be rigidly rotating and chemically homogeneous as a result of the barotropic instability and horizontal turbulence (Zahn 1975, 1992; Chaboyer & Zahn 1992). The uncertain parameters for the mixing and angular momentum transport efficiencies were adjusted to reproduce the observed nitrogen and helium enrichment of massive stars during central hydrogen burning (see Heger et al. 2000 for details).

Magnetic fields were not considered here since their efficiency in redistributing angular momentum by magnetic torque (and mixing by magnetic instabilities) inside stars is still very controversial (e.g., Spruit & Phinney 1998; Spruit 1998 vs. Livio & Pringle 1998) and no reliable prescriptions exist yet. For more details on the progenitor model and the input physics, we refer the reader to Heger (1998) and Heger et al. (2000). If magnetic fields are strong, the angular velocity between the core and the surface may couple during most evolutionary phases, leading to much smaller core rotation rates than found by Heger et al. (2000). In the model for the evolution of an internal stellar magnetic field by Spruit & Phinney (1998), the core rotation decouples from the surface only *after* central carbon depletion. The cores resulting from their calculation carry far too little angular momentum to explain the observed rotation rates of young pulsars (Marshall et al. 1998), and thus Spruit & Phinney (1998) have to employ another mechanism to spin them up again. Livio & Pringle (1998) instead find that the coupling between core and envelope due to magnetic fields should be far less than assumed by Spruit & Phinney (1998), allowing a natural explanation for spin rates of both young pulsars and white dwarfs.

With regard to the relevant physics in core collapse and the neutrino-driven supernova mechanism, the structure of our rotating progenitor is not too different from that of Woosley & Weaver (1995). Figure 2 shows the density and temperature profiles just before collapse for our rotating progenitor and model s15s7b from Woosley & Weaver (1995). Note that beyond a radius of $\sim 3 \times 10^8$ cm, the density of the nonrotating star is roughly a factor of 2 lower than that of the nonrotating Woosley & Weaver progenitor. Pressure equilibrium requires that the temperature at these radii also be lower. Burrows & Goshy (1993) have shown that cores with lower densities are more likely to explode because the ram pressure that prevents the explosion is lower for these cores (see § 4). However, the differences

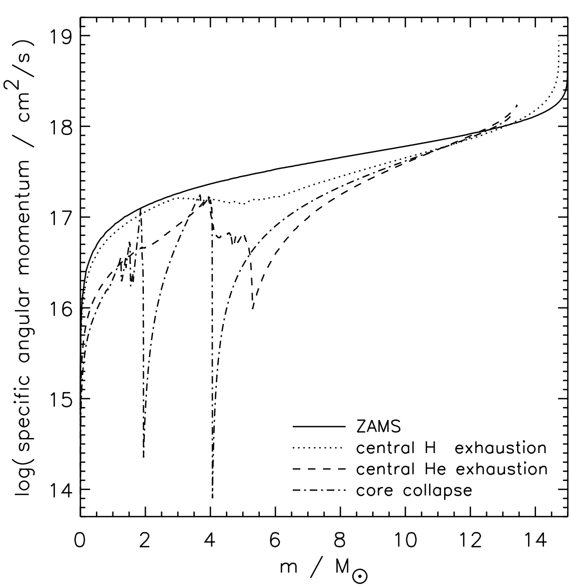

FIG. 1.—Specific angular momentum (shell average; note that the equatorial value of j is 50% higher) of the progenitor model E15B at different evolutionary stages as a function of the interior mass coordinate. The profiles at core hydrogen ignition (ZAMS; *solid line*), central hydrogen depletion (*dotted line*), central helium depletion (*dashed line*), and onset of core collapses (*dash-dotted line*) are given (see also Heger 1998; Heger et al. 2000).

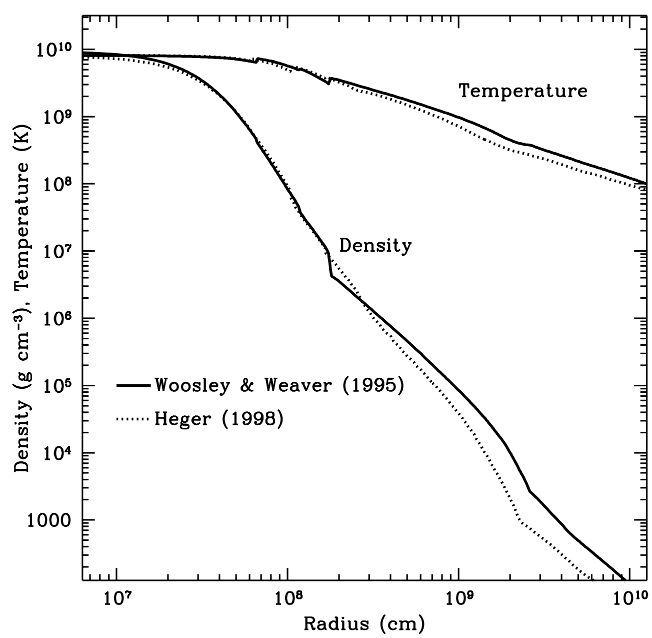

FIG. 2.—Density and temperature profiles for our 15 $M_{\odot}$ rotating progenitor (Heger et al. 2000) and the Woosley & Weaver (1995) progenitor s15s7b. Beyond a radius of 3×10^8 g cm^{-3}, the density of the rotating progenitor drops faster than s15s7b. Pressure equilibrium requires that the temperature decrease faster as well. Although this lower density makes it easier to drive a supernova explosion, its effect is small compared to the effects of rotation.

TABLE 1

ROTATING MODELS

Model Number	Angular Momentum	M_{core} ($M_\odot$)
1	$J_{Heger}(r)$	0.05
2	$J_{Heger}(r)$	0.09
3[a]	$J_{Heger}(r)$	0.05
4[b]	$J_{Heger}(r)$	0.05
5	$0.5J_{Heger}(r)$	0.05
6	0	0.05
7	0	0.09
8[c]	0	0.01

[a] High-resolution run ~32,000 particles.

[b] This model includes an α-disk prescription for the artificial viscosity with α_d set to 0.1 (§ 3).

[c] This simulation uses the progenitor model s15s7b from Woosley & Weaver 1995. All other simulations use the progenitor described in § 2 (Heger et al. 2000).

between these two stars are small enough that they do not change the ultimate features in the core collapse significantly (§ 5).

The angular momentum distribution, on the other hand, does dramatically affect the collapse. The angular velocity profile of our rotating progenitor is shown in Figure 3. We vary the magnitude of this angular momentum in a series of simulations (Table 1). For comparison, we have included the angular velocity profiles of many of the models used by Mönchmeyer & Müller (1989). Rather than obtaining a rotation profile from a rotating progenitor star, Mönchmeyer & Müller (1989) studied arbitrary angular velocity profiles imposed upon a nonrotating progenitor. Their model A closely resembles our rotating progenitor, but most of their models have higher angular velocities, and the effects of rotation are stronger for most of their simulations. In addition, our angular velocity distribution consists of a series of discrete shells that rotate at constant angular velocity, whereas the Mönchmeyer & Müller (1989) models all assume a continuous rotation distribution. These discrete shells are the result of the discrete convective burning regions in the progenitor star. The short convective timescale within these shells causes the material in each shell to reach constant angular velocities (rigid-body rotation). However, shear viscosity does not equilibrate adjacent shells, and thus at the boundaries of convective regions the angular velocity can change abruptly.

For stars where the pressure is only a function of density ($P \propto \rho^\gamma$; e.g., degenerate material), the specific angular momentum is constant along cylinders (Poincaré-Wavre theorem; for a review see Tassoul 1978). Within the rigidly rotating shells of our nearly degenerate precollapse core, the specific angular momentum is indeed constant along both cylinders and shells. In Figure 3, the angular velocity is roughly constant out beyond 6×10^7 cm where the star is no longer degenerate. At the edges of the convective regions, strong gradients of entropy and composition occur. At these boundary layers the pressure is clearly not a function of density alone (Fig. 4) and the Poincaré-Wavre theorem does not apply. Therefore, the cylindrical rotation law does not need to be constant across these boundary layers. We do not expect the specific angular momentum to remain constant along cylinders there, and it does not. In fact, because convection transports the angular momentum in these shells (and not through these shells), we expect the discrete rotation velocities in the shells that we observe.

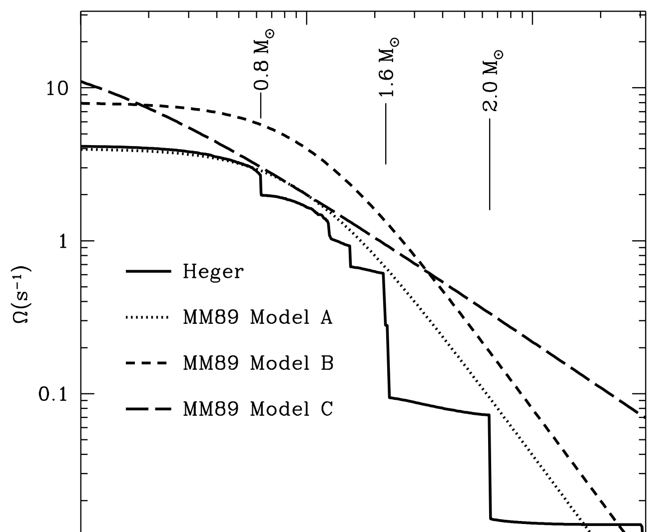

FIG. 3.—Angular velocity profile for our rotating model as well as the prescriptions used in the models of Mönchmeyer & Müller (1989). Except for model A, the models of Mönchmeyer & Müller (1989) are rotating more rapidly than our models, and the effects of rotation on our collapse simulations are much less than most of their simulations. Also note that the angular velocity distribution is a series of step functions. This is because subsequent convection regions tend to equilibrate the angular velocity and only at convective boundaries does the angular velocity change significantly.

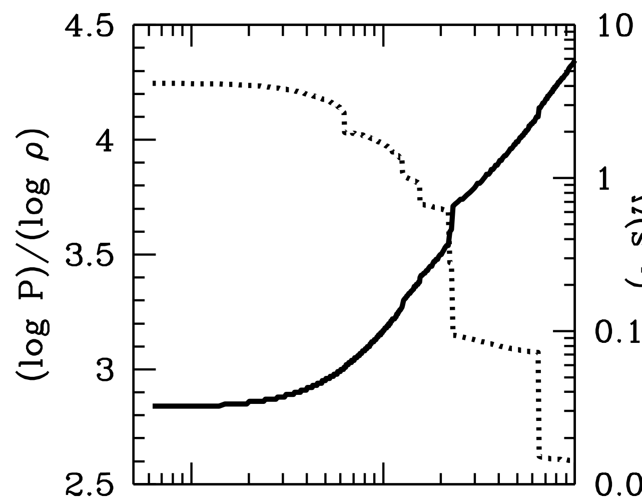

FIG. 4.—log P/log ρ as a function of radius (*solid line*). For stars where the pressure is only a function of density ($P \propto \rho^\gamma$; e.g., degenerate material), the specific angular momentum is constant along cylinders (for a review see Tassoul 1978). Where this does not occur, that is, where log P/log ρ is not constant, this constraint on the angular momentum is no longer true. Note that in the degenerate core, our angular momentum profile (*dotted line*) is constant (which is a sufficient condition for constant cylindrical rotation) and the angular velocity does not vary until much beyond the radius at which pressure is solely a function of density.

How does the distribution of the angular velocities effect the core collapse? For the low rotation speeds used in our simulations, our discrete distribution produces an initial collapse that agrees well with the results achieved using a continuous angular velocity distribution of comparable magnitude (model A) from Mönchmeyer & Müller (1989). This does not mean that all angular momentum distributions of roughly equal magnitude will yield similar core-collapse bounces (e.g., model D from Mönchmeyer & Müller 1989 actually produces an explosion along the equatorial region). Our results only describe the effects of rotation using the angular momentum distribution in the current stellar evolution models (Heger et al. 2000).

3. NUMERICAL TECHNIQUES

For our simulations, we use the smooth particle hydrodynamics (SPH) core-collapse code originally described in Herant et al. (1994) and Fryer et al. (1999). This code models the core collapse in two dimensions continuously from collapse through bounce and ultimately to explosion. The neutrino transport is mediated by a single energy flux limiter. Beyond a critical radius, defined by $\tau = 0.1$, a simple "lightbulb" approximation for the neutrinos is invoked, which assumes that any material beyond that radius is bathed by an isotropic flux equal to the neutrino flux escaping that radius. We use all of the neutrino production and destruction processes discussed in Herant et al. (1994) *except* electron scattering because our neutrino transport algorithm overestimates its effect. The equation of state is identical to that of Herant et al. (1994), which uses a patchwork of equations of state and nuclear burning approximations. At low densities, we use the equation of state by Blinnikov, Dunina-Barkovskaya, & Nadyozhin (1996) with a nuclear statistical equilibrium routine by Hix & Thielemann (1996) for temperatures beyond 5×10^9 K. At high densities, we use the equation of state by Lattimer & Swesty (1991). We implement gravity assuming that the mass distribution is spherical. Assuming a spherical mass distribution also allows us to easily implement general relativity fully into the equations of motion using the technique described by van Riper (1979). This treatment includes both the relativistic modifications to the energy equation and time dilation. We further redshift the neutrino energies as the neutrinos climb out of the core's potential well. However, by assuming spherically symmetric gravity, we introduce errors into the simulations of our fastest rotating stars as their cores flatten. During collapse and bounce, this error is less than 5%–10%, but at late times when the neutron star has cooled, this error rises. However, at these late times, most of the action occurs in the convective region where spherical symmetry is still reasonably accurate (within 10%). During the core collapse and bounce, we believe the effects of general relativity are more important. For our slower rotating stars, these errors decrease dramatically.

Our two-dimensional simulations assume cylindrical symmetry about the rotation axis, modeling a full 180° wedge with a reflective boundary around the symmetry axis. The inner 0.01 $M_\odot$ is also modeled as a reflective boundary that collapses along with the star as described in Herant et al. (1994). Because the progenitor models did not account for centrifugal acceleration, we had to artificially add 0.04 $M_\odot$ to the inner core to induce a collapse (hence, the inner core has an effective mass of 0.05 $M_\odot$). We also ran a set of simulations with 0.08 $M_\odot$ added to the core, but the results did not change (Table 2). For most of our simulations, we use $\sim$9000 particles with a resolution in the convection parts of the star of roughly 2°. We have run one model with $\sim$32,000 particles (twice the resolution), and the results do not change significantly (Table 2).

The initial angular momentum distribution of the progenitor (see § 2; Heger et al. 2000) is mapped onto the two-dimensional grid of particles assuming that the rotation axis is identical to the symmetry axis. Each particle, *i*, is

TABLE 2

ROTATING MODELS

Model	$T_{\rm exp}$[a] (s)	$E_{\rm exp}$[b] (10^{51} ergs)	$M_{\rm rem}$[c] ($M_\odot$)	Explosion Asymmetry: $r^{\rm pole}_{\rm shock}/r^{\rm equ}_{\rm shock}$	Explosion Asymmetry: $V_{\rm pole}$, $V_{\rm equ}$	Rotation[d] (ms)	Ejecta[e] ($M_\odot$): $Y_e < 0.49$	Ejecta[e] ($M_\odot$): ^{56}Ni
1	0.5	0.95, 0.5	1.2, 1.5	1.4	13, 5.1	260, 1.8	0.60, 0.30	0.15
2	0.5	1.2, 0.5	1.2, 1.5	1.3	12, 6.1	140, 1.7	0.56, 0.25	0.2
3[f]	0.5	...	1.2, ~1.5	1.1	12, 5.3	770, 1.8	0.48, 0.18	0.2
4	0.5	1.5, 0.7	1.1, 1.3	1.3	12, 5.5	70, 1.9	0.45, 0.25	0.2
5	0.4	1.9, 1.3	1.2, 1.3	1.2	12, 9.0	260, 1.9	0.50, 0.40	0.3
6	0.2	2.1, 1.5	1.1, 1.2	1.04	8.0, 7.7	...	0.36, 0.25	0.3
7	0.2	2.2, 1.6	1.1, 1.2	1.06	9.7, 9.2	...	0.35, 0.25	0.3
8	0.2	2.5, 1.9	1.1, 1.2	...	...	...	0.23, 0.1	0.3

[a] The explosion time is the time from bounce until the shock has reached 2000 km.

[b] The explosion energy is given as both the net change in energy for the ejected material (see Fryer 1999) and the kinetic energy at infinity.

[c] The two values for remnant mass are before and after fallback.

[d] The rotation period of the neutron star at the end of the SPH simulation (when the star is still rather large) and after the neutron star has cooled assuming no angular momentum is lost.

[e] The first column gives the amount of neutron-rich material ejected both before and after fallback. The second column gives the total nickel mass ejected.

[f] We have only run the high-resolution simulation to explosion (first $\sim$0.5 s) and cannot reliably estimate the explosion energy. Hence, we cannot get a firm estimate on the fallback, but a few tenths of a solar mass of material is likely. The asymmetry in the explosion is not as large because we have not followed the explosion as long. However, the asymmetry in the velocities is the same factor of 2 that we see in the low-resolution runs.

TABLE 3

ONE-DIMENSIONAL EXPLOSION SIMULATIONS

Model	Piston Location ($M_\odot$)	Piston Alpha (artificial part)	Piston Energy[a] (10^{51} ergs)	Artificial Piston Energy[a] (10^{51} ergs)	Explosion Energy[b] ($M_\odot$)	Fallback ($M_\odot$)	Remnant Mass ($M_\odot$)	^{56}Ni Ejected
1[c]......	1.10	0.0017	1.30	0.30	0.52	0.30	1.40	0.18
1.......	1.145	0.004	1.03	0.15	0.48	0.26	1.40	0.16
1.......	1.19	0.01	0.89	0.08	0.45	0.24	1.43	0.13
1.......	1.24	0.017	0.76	0.05	0.40	0.23	1.47	0.10
1.......	1.29	0.035	0.63	0.04	0.34	0.21	1.50	0.06
6.......	1.05	0.002	1.43	0.23	0.67	0.24	1.29	0.21
6.......	1.10	0.03	1.35	0.08	0.73	0.16	1.26	0.24
6.......	1.145	0.05	1.27	0.05	0.72	0.14	1.28	0.22
6.......	1.19	0.07	1.09	0.05	0.64	0.15	1.34	0.18
6.......	1.24	0.1	0.97	0.03	0.60	0.15	1.39	0.14
6.......	1.29	0.12	0.80	0.03	0.49	0.16	1.45	0.07
6[d]......	1.10	0.03	1.34	2.31	0.73	0.15	1.25	0.24
6[d]......	1.10	0.04	1.41	2.38	0.80	0.15	1.25	0.24
6[d]......	1.10	0.10	1.74	2.71	1.13	0.13	1.23	0.27
6[d]......	1.10	0.17	2.05	3.02	1.44	0.11	1.21	0.29
6[d]......	1.10	0.19	2.13	3.10	1.52	0.10	1.20	0.29

[a] Integrated work of the piston.
[b] Kinetic energy (of the ejecta) at infinity ($\sim$1 yr after explosion), assuming expansion into empty space.
[c] At 18.5 s after core collapse the innermost 0.2 $M_\odot$ above the piston were removed from the grid and the new piston radius (10^9 cm) was kept constant. The deviation in the piston energy due to this modification is <1%.
[d] Artificial piston is started when Lagrangian mass element reaches its minimum location.

given an initial specific angular momentum: $j_i = (x_i/r_i)j(r_i)$, where r_i and x_i are the particle's radial distance from the center and its distance from the rotation axis and $j(r)$ is the equatorial angular momentum, $j = \Omega r$, given by the E15B progenitor of Heger et al. (2000; see also Fig. 3). We have also set up models using $j_i = 0.5(x_i/r_i)j(r_i)$ and $j_i = 0$. For most of our simulations, we assume that the angular momentum is conserved, which in our two-dimensional SPH code is true simply by holding j_i constant for each particle.[2] The force on the particles, which are rings in our rotationally symmetric simulation, is modified by adding the centrifugal force: $\equiv j_i^2/x_i^3$. By ranging the initial angular momenta of the particles, we can calculate the effects of rotation.

However, in our rotating models, the angular velocity of the matter (v^ϕ) becomes so high that it may rotate 10–100 periods ($P_i = 2\pi x_i/v_i^\phi$) during the course of the $\sim$1 s simulation. In this case, it is likely that viscous forces will facilitate the transport of angular momentum. To estimate the effects of these viscous forces, we have implemented an α-disk viscosity (Shakura & Sunyaev 1973), which is suitable for the disklike structures that develop as the core collapses. We use the shear viscosity tensor from Tassoul (1978) and drop the terms involving a derivative in ϕ (since $\partial X/\partial\phi = 0$ in our rotational symmetry). Using our SPH formalism, the equations from Tassoul (1978) become

$$\frac{Dj_i}{Dt} = \sum_k \alpha_d \bar{c}_s \bar{H}_p \bar{x}\, \frac{\bar{m}}{m_i}\left[\frac{3\Delta(v^\phi/x)}{r_{ik}+\epsilon\bar{h}} + \frac{\bar{x}\Delta(v^\phi/x)}{r_{ik}^2+\epsilon\bar{h}^2} + \frac{\bar{x}\Delta(v^\phi)}{r_{ik}+\epsilon\bar{h}}\right], \quad (1)$$

[2] Because the rotation axis of the simulation is the same as the angular momentum axis, there is no computational angular momentum transport in our Lagrangian code. Each particle is given an angular momentum, and this angular momentum is held constant throughout the simulation.

where $\alpha_d = 0.1 - 10^{-4}$ is the α-disk parameter; $\bar{c}_s$, $\bar{H}_p$, $\bar{x}$, $\bar{m}$, and $\bar{h}$ are the mean values between neighbor particles i and k of, respectively, the adiabatic sound speed, the disk scale height, the distance from the rotation axis, the particle mass, and the SPH smoothing length; $\Delta(v^\phi/x) = (v_i^\phi/x_i - v_k^\phi/x_k)$; $\Delta(v^\phi) = (v_i^\phi - v_k^\phi)$; r_{ik} is the separation of particles i and k; and $\epsilon = 0.1$. The net energy lost by the particles is then added to the particles equally as dissipation energy, which is equivalent to using the dissipation function given in Tassoul (1978). The summation occurs over all of the SPH neighbors of particles for which $P_i < 1$ s. This implementation conserves angular momentum and energy, and the α-disk viscosity gives some insight into the effects of viscous forces.

To follow the progression of the supernova explosion to late times ($\sim$1 yr after core collapse), we convert from our two-dimensional results back into the one-dimensional stellar evolution code KEPLER (Weaver, Zimmermann, & Woosley 1978). This is the same code that has been used to evolve the stars until core collapse (Heger et al. 2000). When the infall velocity reaches about 1000 km s^{-1}, in KEPLER the inner part of the star is cut out and replaced by a "piston" that first moves inward until bounce and then moves outward until it reaches a final position of 10^4 km. In the present work, the first part of the piston movement is taken from the SPH simulation by following the trajectory of a spherical mass shell. This method leads to a systematic underestimate of the energy input because any spherically determined mass shell has matter flowing through it, and although the mean velocities of the exploding matter are matched, for a given spherical mass coordinate, by the spherically determined mass trajectories, total energy in the explosion can be much higher since the kinetic energy flux through the moving shell does not vanish. As the simulation progresses beyond the maximum time from our two-dimensional simulations, we continue the movement of the piston in such a way that it resembles the free movement of a test particle in the gravitational field of a point mass equal to $\alpha_{\rm piston}$ times the mass interior to the piston that reaches zero velocity at the final location of the piston (10^4 km; see above), following the prescription by Woosley & Weaver (1995).

The value of $\alpha_{\rm piston}$ is chosen such that it "smoothly" continues the piston movements obtained from the SPH simulations. This, however, involves some ambiguity (about a factor of 2 in $\alpha_{\rm piston}$, we estimate) since we have no measure to quantify the quality of this extrapolation. The values of $\alpha_{\rm piston}$ we use are given in Table 3. We carry out these extended supernova simulations for a rotating model (model 1; see Table 1) and a nonrotating model (model 6) and for different locations, in mass, of the piston (Table 3). For model 1 we switch to the "artificial" piston 1.9 s after the onset of core collapse, and for model 6 we switch after 1.0 s. The contribution of this artificial continuation of the SPH-derived pistons to the total work of the piston is also given in Table 3: in most cases it is only small, and thus our choice of $\alpha_{\rm piston}$ should not significantly alter our results. We note that during the inward movement of the piston, work of about 10^{51} ergs (for model 1, 1.1 $M_\odot$ piston) is done against the piston by the infall, and thus the work of the piston counting from its minimum location (in radius) is higher by this amount. The piston energies given in Table 3 are the integrated work energies from the beginning of the SPH simulation until ~ 1 yr after the core collapse.

For the nonrotating model 6 we also carry out a series of explosions where we start the "artificial" piston at the minimum location of the piston (as obtained from the SPH simulation) at a mass coordinate of 1.1 $M_\odot$ and for different values of $\alpha_{\rm piston}$. In comparison to the model of the same mass cut but using the artificial piston only after the end of the SPH data, we get the same energies within less than 1%. The explosion energy turns out to be rather insensitive to the value of $\alpha_{\rm piston}$. Because of the above mentioned underestimate of the explosion energy in the one-dimensional simulation, a value of $\alpha_{\rm piston}$ more than 6 times higher ($6^{1/2}$ times higher piston velocity) is necessary to obtain the same explosion energy as in the SPH simulation. By using the results from this series of piston simulations, we can estimate not only the kinetic energies of our supernova explosions but also the amount of fallback and ^{56}Ni ejected (Table 2).

4. COLLAPSE AND CONVECTION

The evolutionary scenario for the current paradigm of core-collapse supernovae begins with the collapse of a massive star ($M_{\rm star} \gtrsim 8\ M_\odot$), which occurs when the densities and temperatures at the core are sufficiently high to cause both the dissociation of the iron in the core (removing energy from the core) and the capture of electrons onto protons, which further reduces the pressure. This sudden decrease in pressure causes the core to collapse nearly at freefall, and the collapse stops only when nuclear densities are reached and nucleon degeneracy pressure once again stabilizes the core and drives a bounce shock back out through the core. The bounce shock stalls at roughly 100–300 km as neutrino emission and iron dissociation sap its energy. It leaves behind an entropy profile that is unstable to convection and sets up a convective region from ~ 50 km out to ~ 300 km (Fig. 5) capped by the accretion shock of infalling material. The convective region must overcome this cap to launch a supernova explosion.

Neutrino heating deposits considerable energy into the bottom layers of the convective region. If this material were not allowed to convect (which is the case for most of the one-dimensional simulations), it would then reemit this energy via neutrinos producing a steady state with no net energy gain. In the meantime, the pressure increases as more material piles up at the accretion shock, and the neutrino luminosity decreases as the proto–neutron star cools and makes it increasingly difficult to launch an explosion. In the "delayed-neutrino" supernova mechanism (Wilson & Mayle 1988; Miller, Wilson, & Mayle 1993; Herant et al. 1994; Burrows et al. 1995; Janka & Müller 1996), convection aids the explosion in two ways: (1) as the lower layers of the convective region are heated, that material rises and cools adiabatically and converts the energy from neutrino deposition into kinetic and potential energy rather than reradiating it as neutrinos; and (2) the material does not simply pile at the shock but instead convects down to the surface of the proto–neutron star, where it either accretes onto the proto–neutron star, providing additional neutrino emission, or is heated and rises back up. Thus, convection both increases the efficiency at which neutrino energy is deposited into the convective region and reduces the energy required to launch an explosion by reducing the pressure at the accretion shock. It appears that nature has conspired to make core-collapse supernovae straddle the line between success and failure, where convection, which for years was thought to be a mere detail, plays a crucial role in the explosion. Thus, it is not surprising that the outcome of the core collapse of massive stars depends upon numerical approximations of the physics, for example, the algorithm for neutrino transport (Messer et al. 1998; Mezzacappa et al. 1998b). It is also not surprising that changes in the progenitor (i.e., rotation, the subject of this paper) can also lead to different outcomes.

For a rotating core collapse, this basic evolutionary history remains the same, but many aspects of the collapse, bounce, convection, and explosion phases change. To determine these variations, we compare a rotating star (E15B from Heger et al. 2000) with its nonrotating counterpart (unless otherwise stated, all quantitative results and figures compare models 1 and 6). First, angular momentum slows the collapse and delays the bounce (Mönchmeyer & Müller 1989; Janka & Mönchmeyer 1989). For our rotating model, the bounce occurred 200 ms into the simulation, a full 50 ms longer than the nonrotating counterpart. For very high angular momenta the central density at bounce can be lower than in a nonrotating star by over an order of magnitude (Mönchmeyer & Müller 1989; Janka & Mönchmeyer 1989), but for the more modest angular momenta from Heger et al. (2000) the central density at bounce drops from 4×10^{14} g cm^{-3} for a nonrotating star to 3×10^{14} g cm^{-3} for the rotating case. This lower critical bounce density occurs because the centrifugal force begins to provide significant support (it increases from 2% to 10% of the gravitational force over the course of the simulation). The resulting bounce shock is weaker and, along the poles, stalls at lower radii than the nonrotating case. Along the equator, where the effective gravity is less, the accretion shock moves much further, and the star quickly loses its spherical symmetry (Fig. 6). About 60 ms after the bounce, the accretion shock of the rotating model is at ~ 160 km for the poles and 300

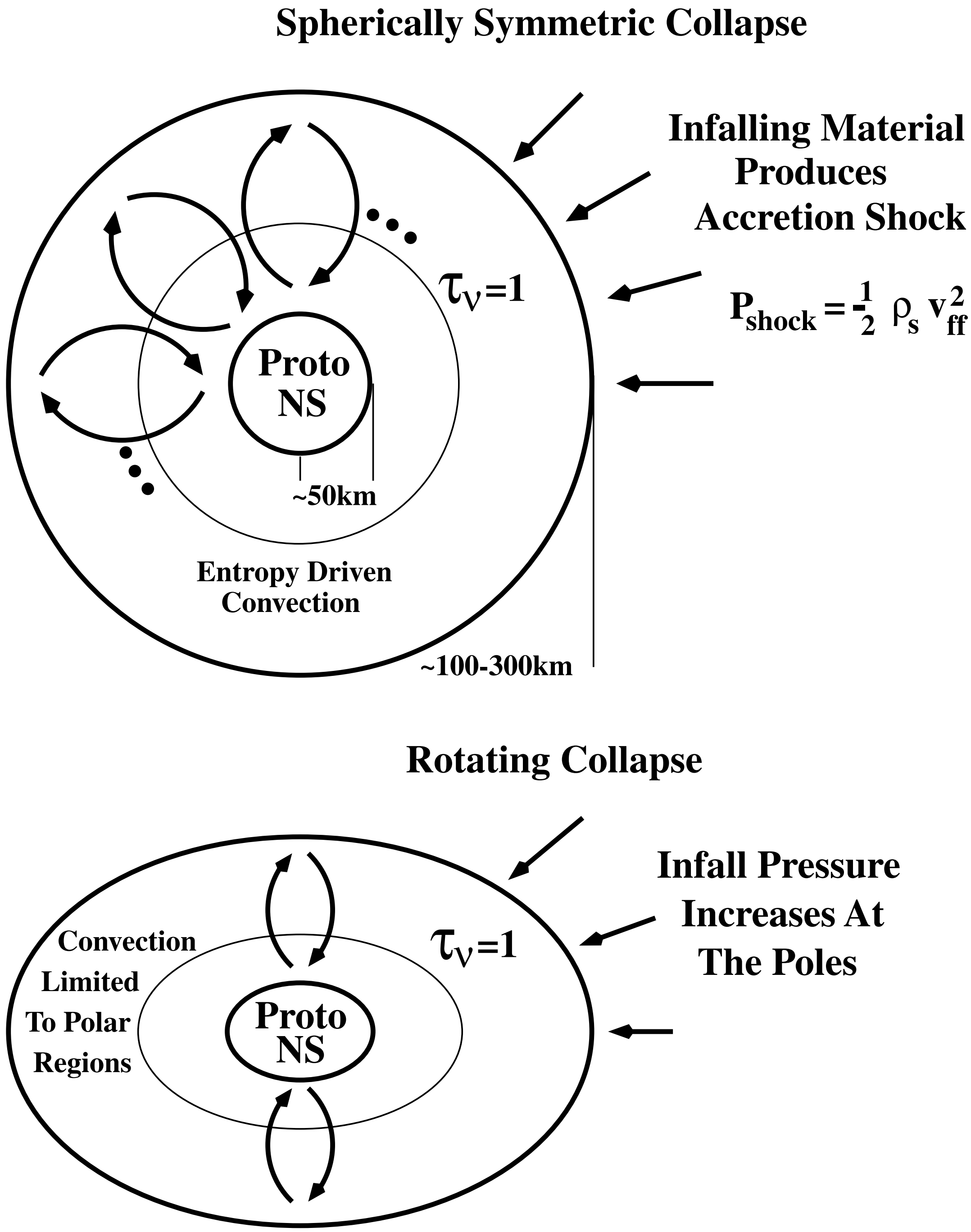

FIG. 5.—Entropy-driven convection has been found to enhance the energy deposition within the accretion shock. As the density of the infalling matter decreases, the convective region is able to push the shock outward, launching a supernova explosion. The proto–neutron star may also convect (Burrows et al. 1981; Keil et al. 1996), increasing the neutrino flux at its surface and the neutrino heating in the convective region. The angular momentum profile in rotating core collapses stabilizes the convection along the equator. $\tau_\nu = 1$ is the radius at which the optical depth of neutrinos is 1. This radius is different for the different types of neutrinos, but for the electron and antielectron neutrinos it extends in the convective region.

km along the equator. At that time, the spherically symmetric accretion shock of the nonrotating star is at ~ 300 km.

The position of the accretion shock, initially set by the position at which the bounce stalls, is important for the success or failure of the convection-driven supernova mechanism because it determines the ram pressure that the convective region must overcome to drive an explosion. Even more important, however, is the entropy profile that is left behind after the bounce shock stalls. Because the bounce is weaker for rotating stars, the angle-averaged entropy decreases with increasing angular momentum (Fig. 7). The entropy in the strong shock limit is $\propto v_{\rm shock}^{1.5}$, and along the equator, where the material is collapsing less quickly, the entropy is much lower (Fig. 8). The steep entropy gradient in supernovae is what seeds the convec-

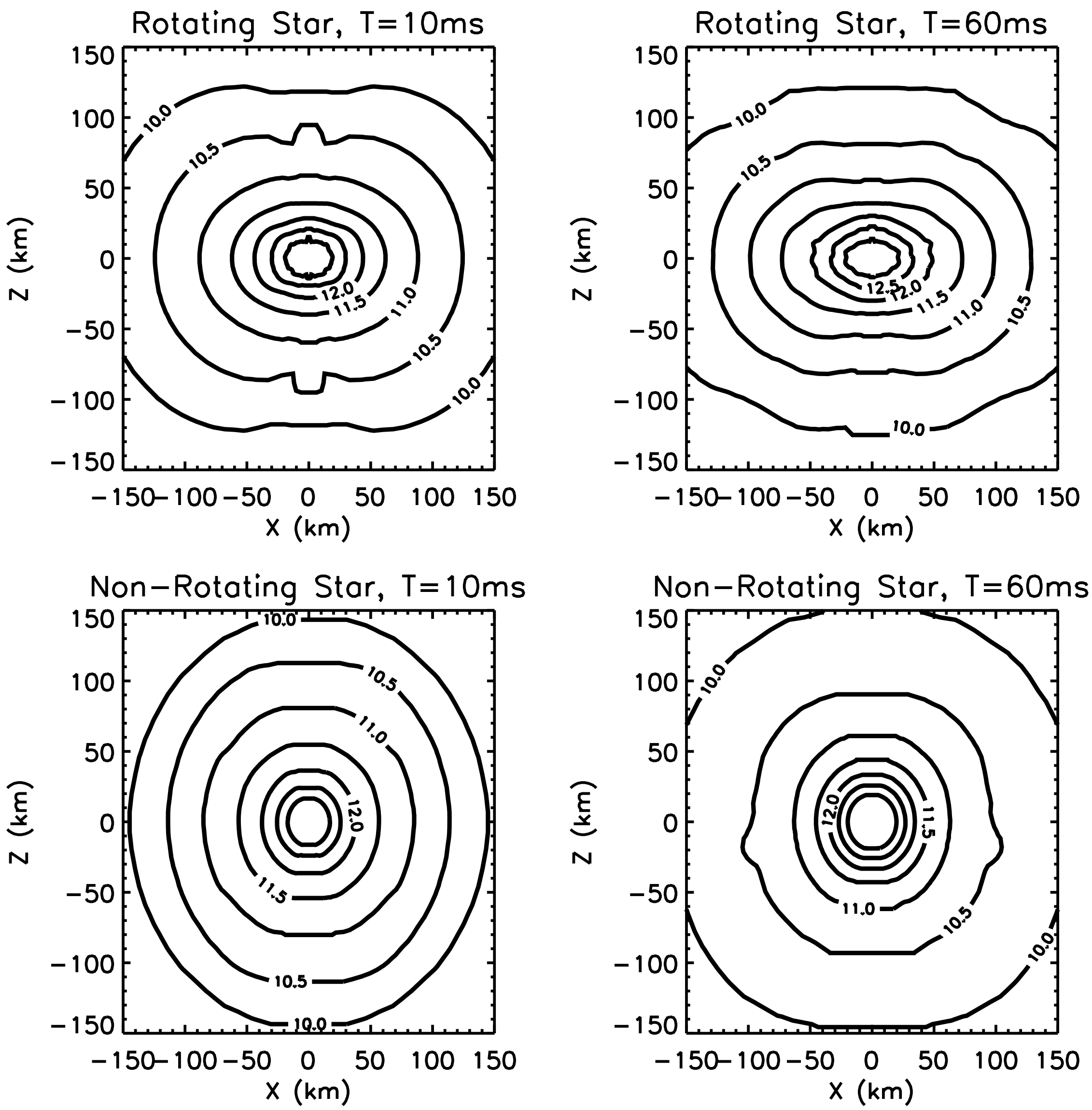

FIG. 6.—Surfaces of constant density (logarithmically spaced) for rotating and nonrotating stars (models 1 and 5) at 10 and 60 ms after bounce. At 60 ms after the bounce, the axis ratio (pole/equator) of the proto–neutron star (densities $\gtrsim 10^{11}$ g cm^{-3}) has dropped to 0.6. At this time, the accretion shock of the rotating model is at ~ 160 and 300 km, respectively, for the poles and the equator. In the case of a nonrotating star, the spherically symmetric accretion shock is at ~ 300 km.

tion, and the shallower gradients in the collapse of rotating stars lead to much weaker convection and, as we shall see in § 5, weaker explosions.

Rotation further weakens the explosion because the angular momentum profile is stable to convection and constrains convection to the polar regions. This can be understood physically by estimating the change of force on a blob of material as it is slightly raised from a position, r, with given density, ρ, angular momentum, j, and pressure, P, to a new position, $r + \Delta r$, with its corresponding density, angular momentum, and pressure, $\rho + \Delta\rho$, $j + \Delta j$, and $P + \Delta P$. If the blob is allowed to reach pressure equilibrium in its new surroundings, the acceleration that it feels without rotation is simply $\Delta a = \Delta a_{\rm buo} = g[1 - (\rho + \Delta\rho)/\rho_{\rm blob}]$, where g is the gravitational acceleration and $\rho_{\rm blob}$ is the density of the blob of material after it has expanded/contracted to reach pressure equilibrium. If the change in acceleration is positive, the blob of material will continue to rise and that region is convectively unstable. This gives us the standard Schwarzschild-Ledoux instability criteria (Ledoux 1947): a region is unstable if $(\partial\rho/\partial r) < (\partial\rho/\partial r)_{\rm adiabat}$, or, for constant composition, $\partial S/\partial r < 0$. If there is an angular momentum gradient, however, the net force on the blob becomes

$$\Delta a = g\left(1 - \frac{\rho + \Delta\rho}{\rho_{\rm blob}}\right) + \frac{j_{\rm blob}^2 - (j + \Delta j)^2}{(r + \Delta r)^3}\ , \qquad (2)$$

where $j_{\rm blob} = j$. The corresponding Solberg-Høiland instability criterion in the equatorial plane is (Endal & Sofia 1978)

$$\frac{g}{\rho}\left[\left(\frac{d\rho}{dr}\right)_{\rm adiabat} - \frac{d\rho}{dr}\right] - \frac{1}{r^3}\frac{dj^2}{dr} > 0\ . \qquad (3)$$

If the angular momentum increases with increasing radius as it does for our core-collapse models (Fig. 9), then the

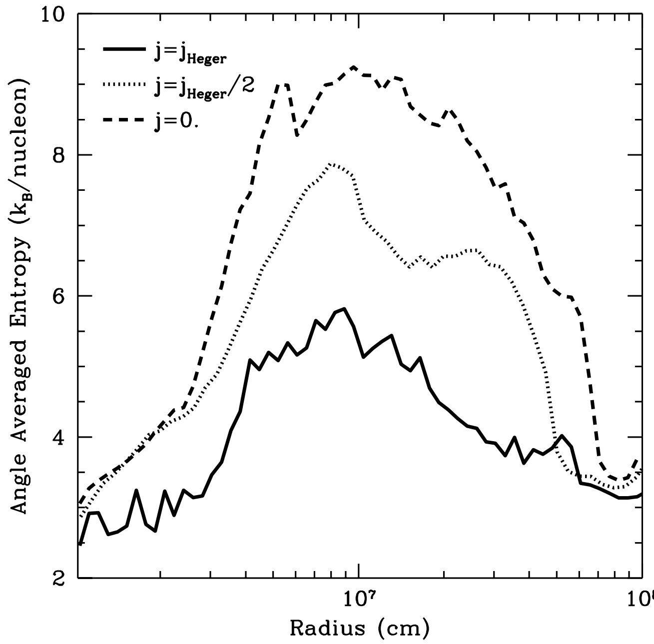

FIG. 7.—Angle-averaged entropy for stars with a range of initial angular momentum (models 1, 5, and 6) 60 ms after bounce. As the angular momentum increases, the entropy profile becomes shallower. The entropy gradient seeds the convection that must overcome the ram pressure of the accretion shock to produce a supernova explosion. Convection in the case of rotating stars will be less vigorous, and these stars will explode later.

entropy gradient must overcome the angular momentum gradient to drive convection. A large negative entropy gradient does not develop in the equatorial region, and, because the angular momentum gradient is very large in the equator, no convection occurs in the equatorial region (Fig. 10). Convection can occur in the polar region, where the magnitude of the negative entropy gradient is much larger and the angular momentum gradient is lower by a factor of 10 or more. The overwhelming effect of rotation on supernova models is this constraint on the convection that causes weaker, asymmetric explosions.

5. EXPLOSIONS AND COMPACT REMNANTS

Because convection is limited in rotating models, the convective region has less energy and is unable to overcome the pressure at the accretion shock as early as in nonrotating models, which explode within 200 ms of bounce. However, at later times (500 ms after bounce), when the density of the infalling material decreases, rotating models are able to launch an explosion, but the explosion occurs later and the proto–neutron star accretes slightly more mass (Fig. 11; Table 2). The final compact remnant mass, however, depends upon the amount of material that falls back onto the proto–neutron star. By mapping our explosions back into one dimension, we can estimate the amount of fallback and the observed explosion energy (Table 2). The masses in Table 2 are baryonic masses. Gravitational masses, which can be compared to observations, are typically $\sim 10\%$ lower. Mass estimates from observations of close binaries predict gravitational masses for stars without hydrogen envelopes to be $\sim 1.4\ M_{\odot}$. Even including fallback, our nonrotating models produce remnants with masses that are much lower than those observed. In addition, the explosion energies are too low to explain all of the observations. Indeed, because of the uncertainties in other aspects of the supernova simulation (e.g., neutrino physics, equation of state, progenitors), the quantitative results from these simulations are likely to vary as a more accurate input physics becomes available. Although we can make no quantitative prediction of the neutron star mass distribution at birth, our calculations indicate clear trends caused by rotation in neutrino-powered supernovae: rotating stars produce weaker explosions and more massive remnants.

Not only are the explosions weaker for rotating stars, but since the convection is constrained to the poles, the explosion is stronger along the poles (Figs. 12, 13, and 14). At the end of the simulation, ~ 1.5 s after bounce, the shock radius is 1.4 times farther out along the pole than along the equator for our rotating star (Table 2). The mean velocity of the shocked material being ejected at the end of the simulation (2/3 of the explosion energy is still thermal) is 13,000 km s^{-1} along the pole and only 5100 km s^{-1} along the equator! The maximum velocity along the pole can be as high as 18,000 km s^{-1}. These results must be taken with some degree of caution, since the axis of symmetry lies along the polar axis, and some of this asymmetry could be due to numerical artifacts. However, if we compare these results with those for a nonrotating star, we are encouraged that this asymmetry is real. In all four simulations of our rotating stars, the mean ejection velocities vary by a factor of 2, whereas for the two simulations of nonrotating stars, the shock radius is only 4% farther out along the poles, and the mean polar and equatorial velocities are 8000 and 7700 km s^{-1}, respectively (maximum velocities are as high as 20,000 km s^{-1}). The variations from pole to equator in the nonrotating simulations are likely to be caused by the position of the rising bubbles and downflows during the explosion. Even if these variations were all due to numerical artifacts (it could be due to convection plumes and hence physical), it appears that numerical artifacts can account for only 10% variations in the velocities, and the large asymmetry in the rotating simulations are likely to be real. By constraining the convection to the poles, rotating models produce more than a factor of 2 asymmetry in the explosion. Although we could not follow the explosion in our high-resolution run, a factor of 2 asymmetry in the explosion velocity already appears 0.4 s after bounce (Fig. 14; Table 2). Again, we stress that the quantitative numbers presented here will change with future supernova models (in this case, moving to three dimensions may cause the biggest differences), and the trend of increasing asymmetry with rotation will probably persist.

Neutrino luminosities for rotating and nonrotating stars are plotted in Figure 15. The nonrotating core has a much larger μ and $\tau(\nu_x)$ neutrino luminosity, especially just after bounce. This is because the nonrotating core compresses more and, at the μ and τ neutrinosphere, the temperature is over a factor of 1.5 times higher than that of the rotating core. The large dependence of neutrino emission on temperature (the luminosity from pair annihilation is proportional to T^9) causes this small change in temperature to have large effects on the neutrino luminosity. Also, bear in mind that beyond 0.2 s after bounce, the regions just above the proto–neutron star look dramatically different. The nonrotating star has already launched an explosion, leaving a hot, bare proto–neutron star that continues to cool by emitting neutrinos. The rotating core is still convecting, and its neutrinosphere is farther out. These differences are more

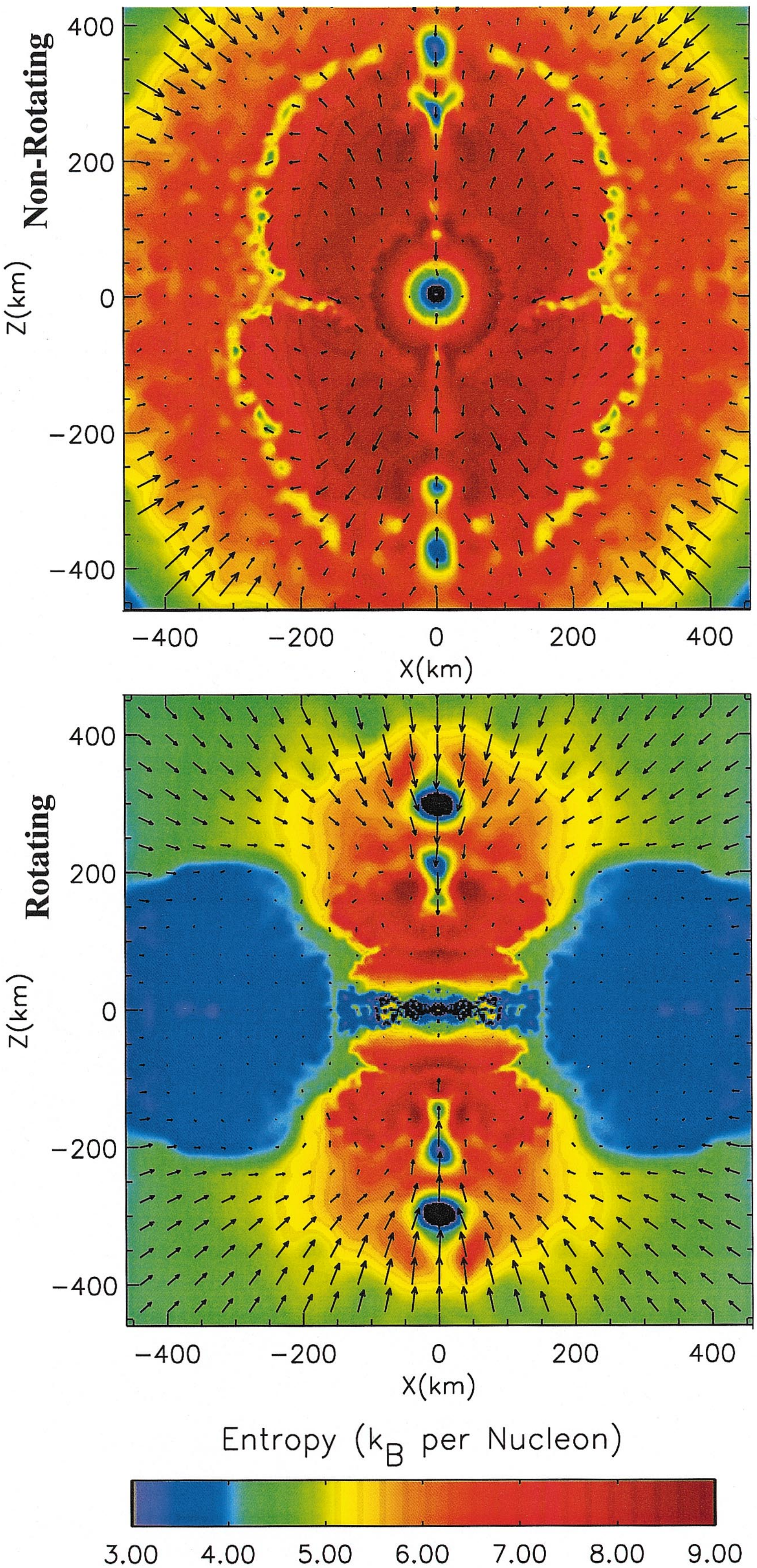

FIG. 8.—Entropy distribution ~50 ms after bounce for nonrotating and rotating cores. For the rotating model, the large increase in entropy caused by the bounce shock is limited to the polar region. The overlying velocity vectors show that the nonrotating model has already developed vigorous convection.

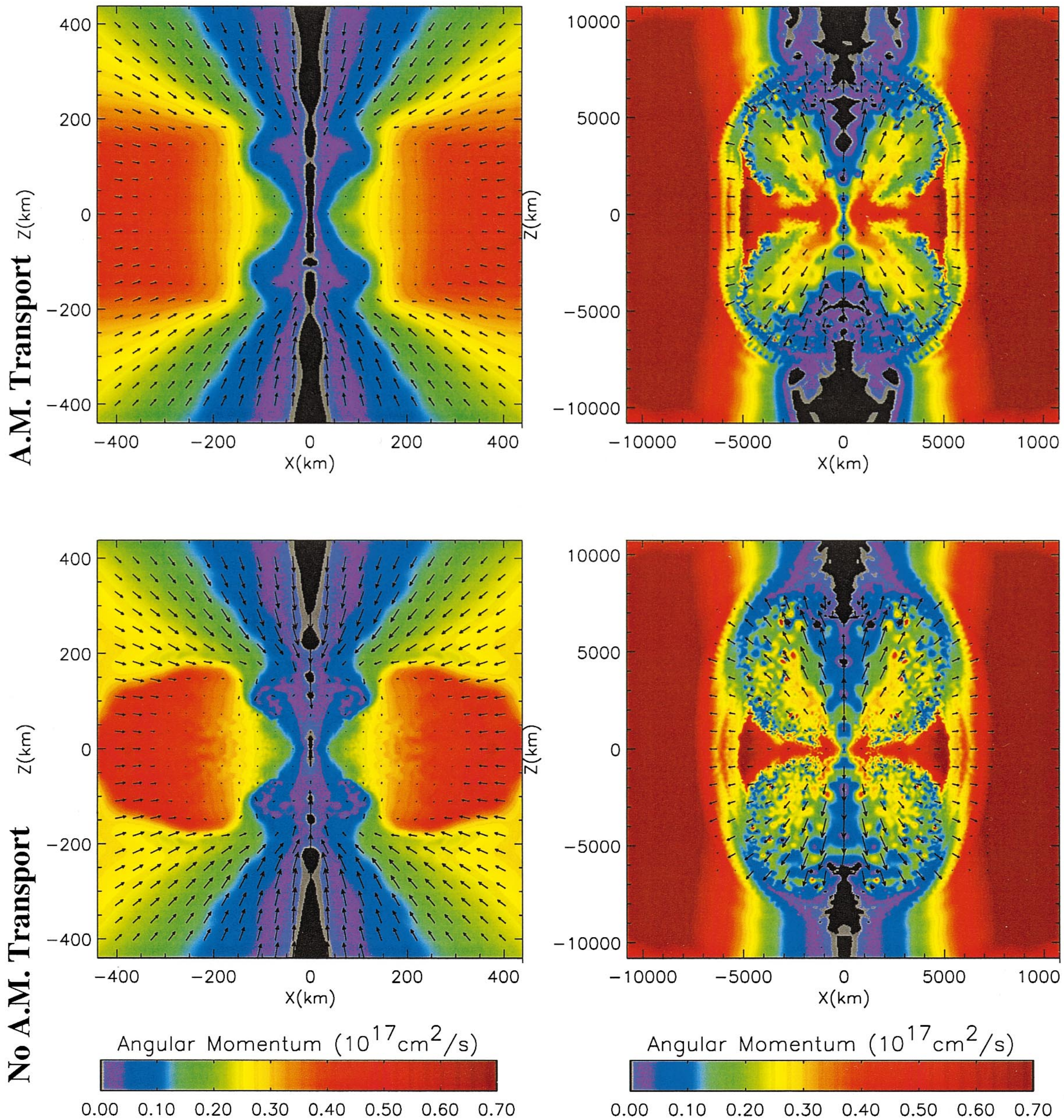

FIG. 9.—Angular momentum distribution $\sim$50 ms and at the end of the simulation for models 1 and 4. The large angular momentum gradient along the equator must be overcome to drive convection in the equatorial region. Angular momentum transport in model 4 smoothes the angular momentum profile, but because the rotation period is still roughly 0.1 s by the end of the simulation, the amount of angular momentum in the two models is similar. At late times, both models show the presence of a disk around the proto–neutron star.

easily seen in a plot of neutrino energies (Fig. 16). If we instead compare the two cores before the launch of the supernova explosion in the nonrotating case (the first 0.2 s), the neutrino emission between the two models agrees much better. The small differences in the neutrino emission at these early times will not produce significant differences in the explosions between rotating and nonrotating stars. We infer no net asymmetry in the neutrino luminosity. But because of our coarse resolution and the rapid time variation of the neutrino luminosity as bubbles rise above the neutrinosphere, asymmetries of $\sim$20%–30% could be hidden in our data and we can neither confirm nor rule out the asymmetric neutrino emission seen by Janka & Mönchmeyer (1989).

Rotating progenitors produce rotating compact remnants. Table 2 lists the spin period of the compact remnant assuming solid-body rotation both at the end of the simulation before the neutron star has cooled and after it has cooled to a 10 km neutron star. Even for model 4 (Fig. 9; Table 2), which includes the transport of angular momentum using an α-disk prescription, at the end of the simulation the angular momentum in the proto–neutron star is sufficient to produce a millisecond pulsar. This is because, at the end of our SPH simulations, the proto–neutron star is still large and is not rotating rapidly. Hence, viscous momentum transport does not have an opportunity to remove the angular momentum from the core. As the neutron star contracts and the spin increases, the neutron star will lose angular momentum through a wind. Hence, the spin period of the cooled neutron star should be seen as a lower limit. In addition, convection in the cooling proto–neutron star (Burrows, Mazurek, & Lattimer 1981; Keil,

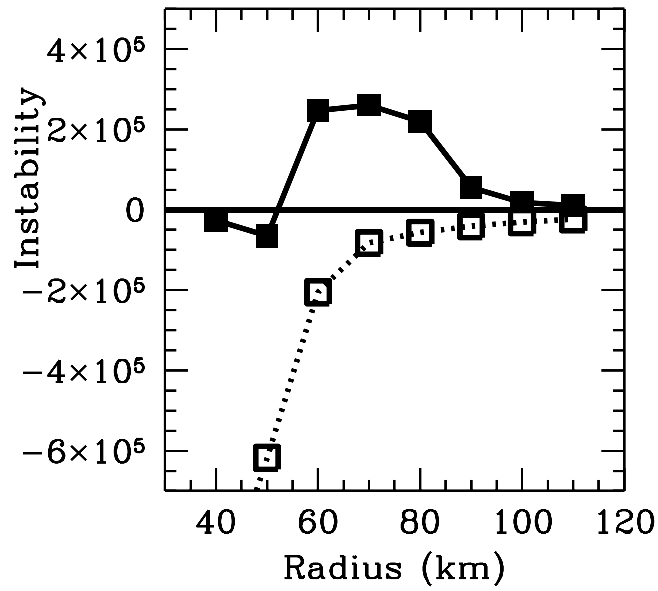

FIG. 10.—Instability parameter (eq. [3]) vs. radius for the polar region (30° cone; *filled squares*) and the equatorial region (30° wedge; *open squares*) in the rotating model 50 ms after bounce. If this instability parameter is less than zero, the material is stable to convection. If it is greater than zero, the material is convectively unstable. The j^2 derivative is 10 times larger in the equator than in the polar region, and there is essentially no entropy gradient in the equatorial region to drive convection. In the polar region, the entropy drops from $8k_B$ per nucleon down to $4k_B$ per nucleon in 30 km, and since the gradient in j^2 is low, strong convection can develop.

Janka, & Müller 1996) will increase the efficiency of the viscous transport of angular momentum. Even in the absence of any wind, gravitational radiation limits the spin period to ∼3 ms (Lindblom, Mendell, & Owen 1999). Fallback may be able to spin up the neutron star but will not be able to exceed the limit from gravitational radiation because the accreting material heats the neutron star to temperatures where gravitational radiation will effectively remove the angular momentum (Fryer, Colgate, & Pinto 1999).

A common problem to all core-collapse simulations that produce explosions is the large amount of neutron-rich ejecta. Although the amount of material ejected with extremely low electron fraction ($Y_e < 0.4$) decreases from 1.2×10^{-3} $M_\odot$ for the nonrotating model to 1.1×10^{-5} $M_\odot$ for the rotating case, the delayed explosion gives more time for neutrino emission to deleptonize the ejecta, and the amount of mildly neutron-rich material ($Y_e < 0.49$) actually increases: from 0.36 $M_\odot$ for the nonrotating model to 0.60 $M_\odot$ for the rotating models. This effect is smaller in the high-resolution run (Table 2). The material that falls back onto the neutron star will be mostly comprised of this neutron-rich material. However, even assuming that only neutron-rich material falls back onto the neutron star, more than 0.1 $M_\odot$ of neutron-rich material is ejected, more than an order of magnitude greater than the 10^{-2} to 10^{-3} $M_\odot$ constraint from nucleosynthesis (Trimble 1991). Clearly, rotation is not the solution to the nucleosynthesis problem, and our supernova simulations still lack some crucial physics (probably in either the neutrino transport or neutrino cross sections).

6. IMPLICATIONS

Rotation limits the convection in core-collapse supernovae, both by weakening the shock and by constraining the convection to the polar regions. Because of these constraints, the convective region takes longer to overcome the accretion shock, and the explosion occurs at later times and is less energetic. The resultant compact remnants of the collapse of rotating stars are more massive. For higher mass progenitors, the density of the infalling material and hence the shock pressure increase (Burrows & Goshy 1993). Because of their limited convection, rotating cores are less likely to overcome the accretion shock, and the critical mass limits for black hole formation (both from fallback and direct collapse) are likely to be lower than those predicted for nonrotating stars (see Fryer 1999). Hence, rotating stars are more likely to collapse directly to form a black hole. The direct collapse of rotating massive stars is becoming increasingly important as a gamma-ray burst mechanism (MacFadyen & Woosley 1999) where the rotation is required to produce the disk that powers a gamma-ray

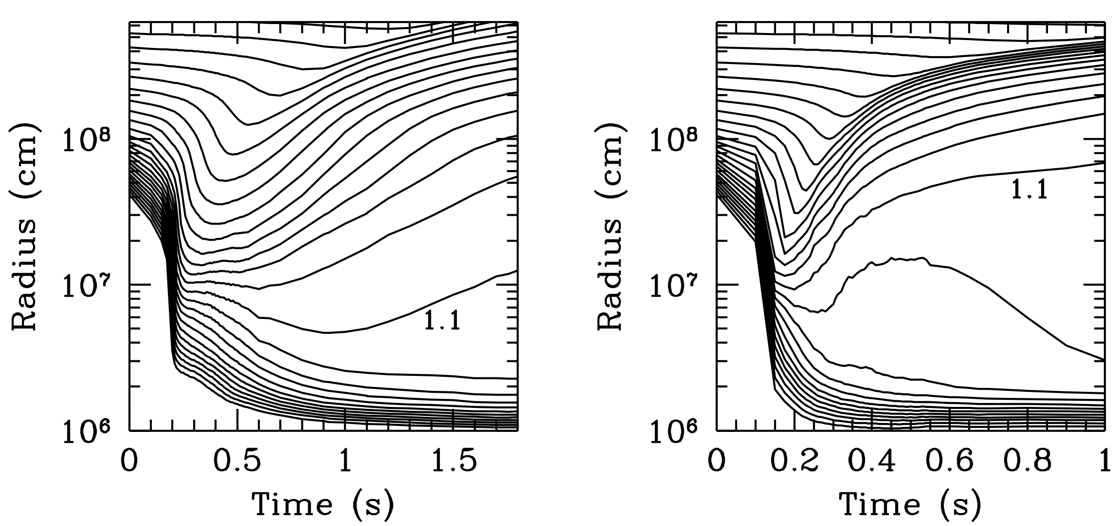

FIG. 11.—Mass trajectories vs. time for the rotating (*left*) and nonrotating (*right*) models (models 1 and 6). Note that the rotating model explodes much later than the nonrotating case. The mass point that contains 1.1 $M_\odot$ is labeled, and every line marks a change of 0.05 $M_\odot$.

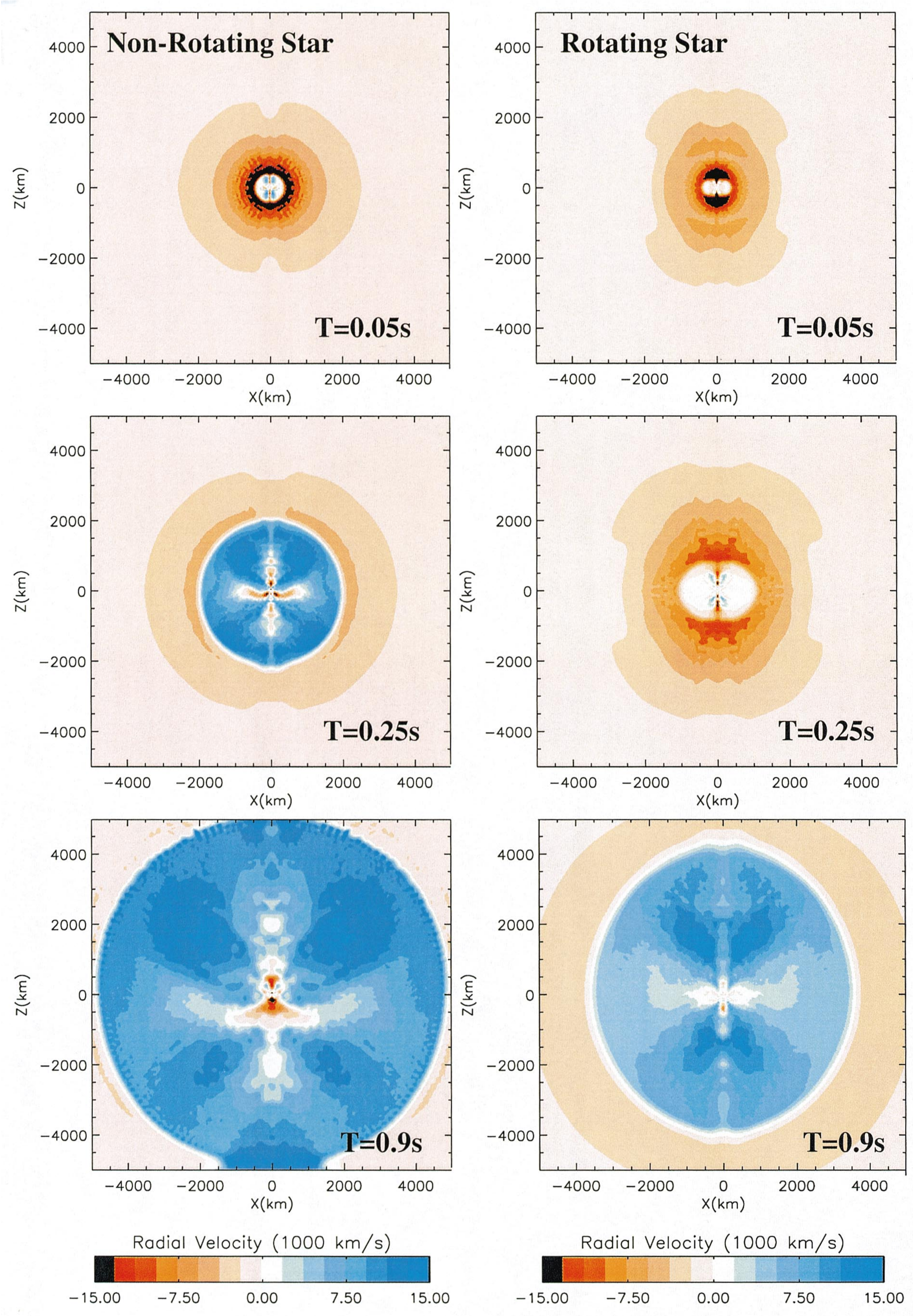

FIG. 12.—Radial velocity distribution of nonrotating and rotating models 0.05, 0.25, 0.5, and 0.9 s after bounce. At 0.9 s, the nonrotating model remains essentially spherical. The asymmetries in the velocities are caused by the buoyant convective bubbles that are driving the explosion. In contrast, the rotating model already shows strong asymmetries in the shock position and velocities.

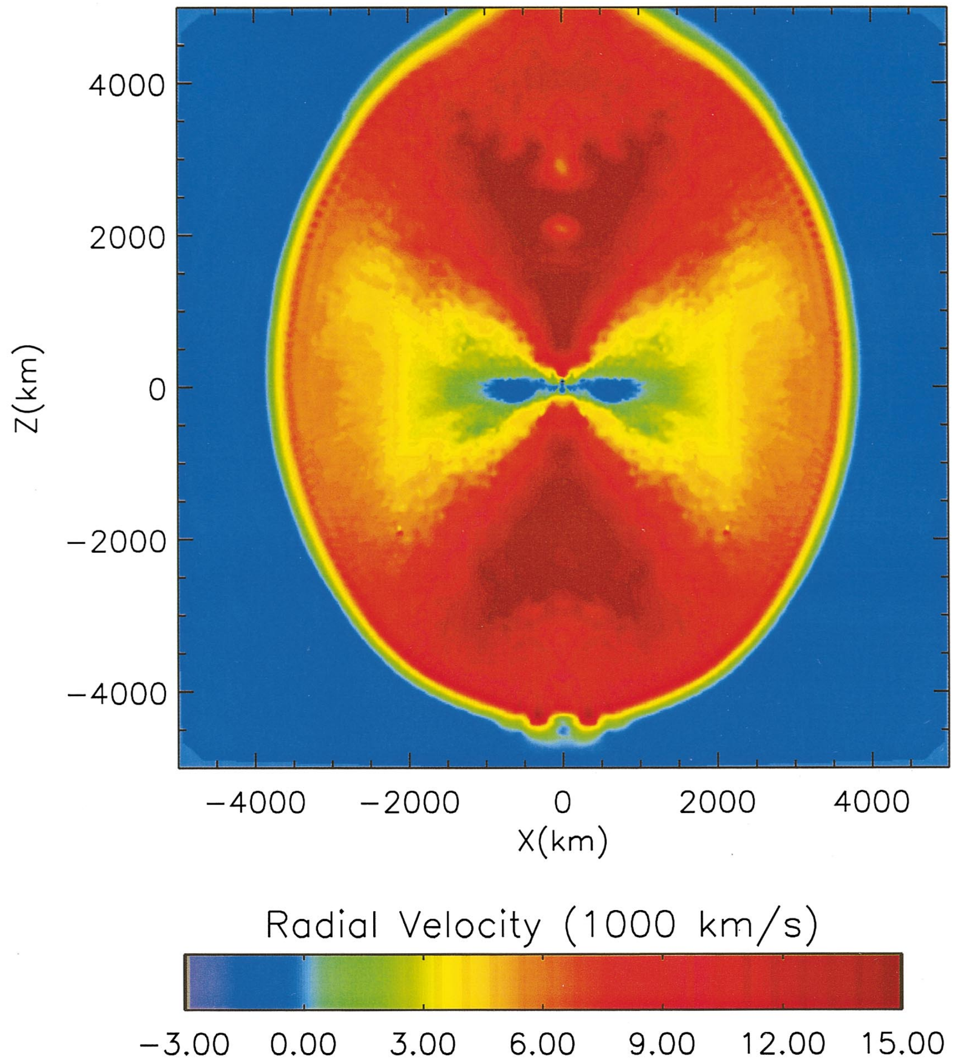

FIG. 13.—Radial velocity distribution of the rotating model (model 1) 1.6 s after bounce. Note the strong jet being driven in the polar region. The momentum asymmetry between the upper and lower poles is 6×10^{39} g cm s^{-1}, which corresponds to a neutron star kick of roughly 30 km s^{-1}.

burst fireball. We expect a range of progenitor mass limits for black hole formation depending on the core rotation. This may help to explain the observed range of black hole systems (Ergma & van den Heuvel 1998). We stress that the uncertainties in the numerical implementation of the physics (e.g., neutrino transport, neutrino cross sections, equation of state, symmetric gravity) limit our ability to make quantitative estimates, and the numbers should be regarded merely as current "best estimates." The trends (e.g., weaker explosions and lower black hole formation limits) are more secure.

If angular momentum were conserved, the rotation periods of neutron stars formed from our progenitor model would be much faster than those expected in nascent neutron stars. However, winds and gravitational radiation will remove much of the angular momentum. The *r*-mode instability found by Lindblom, Owen, & Morsink (1998) can rapidly spin down rotation neutron stars, resulting in the slower observed rotation rates of nascent neutron stars (see Heger et al. 2000). If anything, it will be difficult to explain any rapidly spinning nascent neutron stars.

Not only are the explosions of rotating core collapses weaker, but they are highly asymmetric (roughly a factor of 2 in the mean velocities from pole to equator). Polarization measurements of core-collapse supernovae suggest that most supernovae are polarized (Wang et al. 1996; Wang & Wheeler 1998). In modeling SN 1993J, Höflich et al. (1995) required explosions with asymmetries of a factor of 2, roughly the same asymmetry we see in our simulations, and hence rotation might provide a simple explanation of polarization measurements. These asymmetric explosions also provide a simple explanation for the extended mixing in supernovae. Observations of SN 1987A in X-rays (Dotani et al. 1987; Sunyaev et al. 1987), gamma-rays (Matz et al. 1988), and even in the infrared (Spyromilio, Meikle, & Allen 1990) all push toward extended mixing of iron-peak elements. The matter ejected along the poles, with their much higher velocities, will mix deeper into the star. To determine quantitatively the amount of mixing and polarization produced by the asymmetric explosions of our rotating cores, high-resolution, multidimensional simulations must be run out to late times.

We do not model magnetic fields in our simulations, but we can place some constraints on their importance in the supernova explosion. Thompson & Duncan (1993) have argued against primordial magnetic fields for neutron stars and instead suggest that strong neutron star magnetic fields are produced in dynamos during the supernova explosion

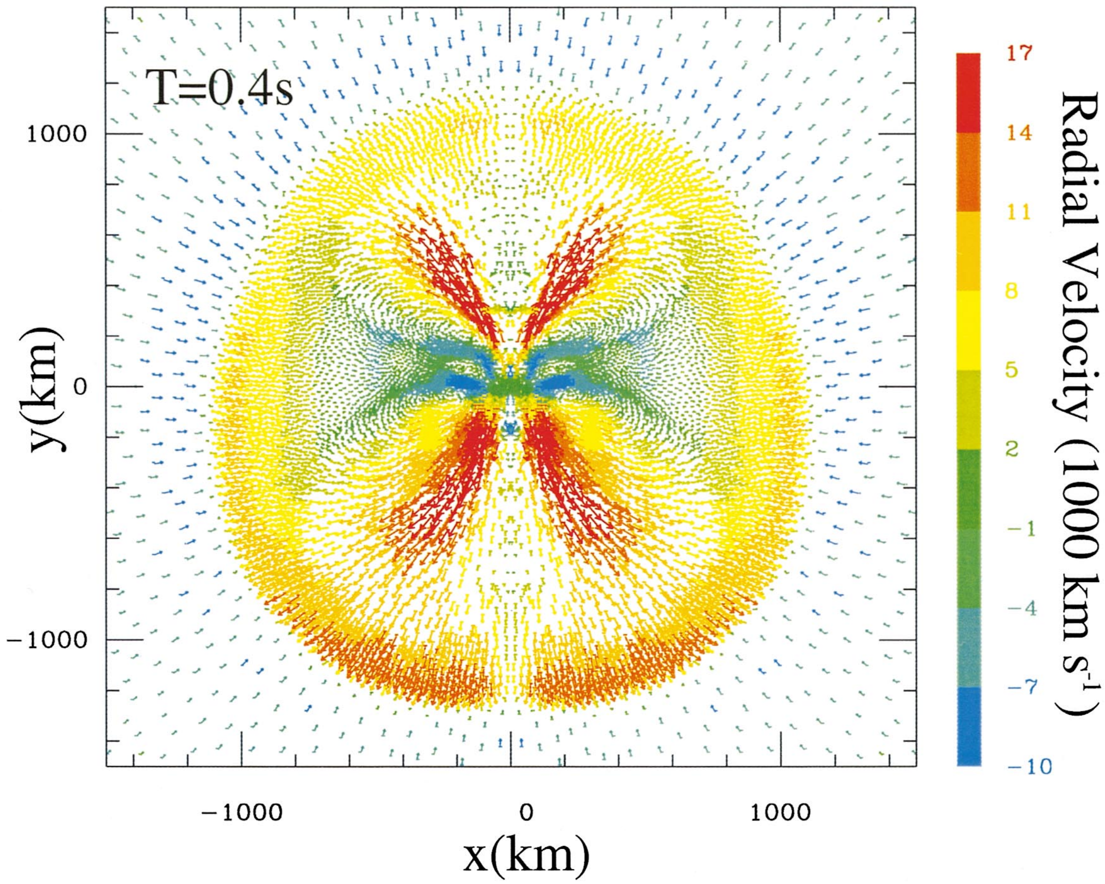

FIG. 14.—Radial velocity distribution of the high-resolution, rotating model (model 3) 0.4 s after bounce. The convective region is just developing into an explosion, and it is already clear that the ejection velocities will become asymmetric. This high-resolution run gets quantitative results (see Table 2) very similar to its low-resolution counterpart (model 1).

itself. They propose a high Rossby number[3] dynamo, which takes advantage of the fast convection velocities, and hence high Rossby numbers of core-collapse supernovae. However, this dynamo requires many convective turnovers ($\tau_{\rm con} \lesssim 10^{-3} t_{\rm exp}$, where $t_{\rm exp}$ is the explosion time) to significantly magnify the magnetic fields. However, for our rotating supernovae, with typical convection length scales of $\sim$400 km and velocities of $\sim$4000 km s^{-1}, the explosion is launched before convection can produce a strong magnetic field. In addition, until the proto–neutron star cools and contracts, the rotation period of the disklike structure is also slow (Table 2), and a rotation-driven dynamo will not occur until after the supernova explosion.

As the proto–neutron star cools and shrinks, however, the Thompson & Duncan (1993) dynamo, driven by Ledoux convection (see Burrows et al. 1981; Keil et al. 1996), is more promising. The strength of this convection is still a matter of debate (Mezzacappa et al. 1998a), but if it is as strong as Keil et al. (1996) predict, magnetic fields in excess of 10^{15} G are obtainable at late times using the convection-driven dynamo of Thompson & Duncan (1993). These magnetic fields will enhance the angular momentum lost in the proto–neutron star wind. But in all of our simulations, this occurs after the launch of the explosion, and the magnetic field would not affect the supernova explosion.

[3] Ro $= P_{\rm rot}/\tau_{\rm con}$, where $P_{\rm rot}$ is the rotation period and $\tau_{\rm con}$ is the convective turnover timescale.

Last, and most speculatively, we come to the topic of neutron star kicks. There is a growing set of evidence that neutron stars are born with high space velocities with a mean magnitude of $\sim$450 km s^{-1} (see Fryer & Kalogera 1998 for a review). Rotation breaks one symmetry, and it is tempting to speculate that it is then easy to break an additional symmetry, causing a net momentum in the ejecta that is nonzero. To balance out the momentum, the neutron star must then have gained some momentum. Indeed, the net momentum of the ejecta along the poles in our simulation is 6×10^{39} g cm s^{-1}. This corresponds to a kick velocity of only 30 km s^{-1}, over an order of magnitude too small to explain the observed pulsar velocity distribution. And this momentum may be entirely a numerical artifact. Asymmetric neutrino emission can also cause neutron star kicks, but we detect no significant neutrino asymmetry. In any event, calculating quantitative results on neutron star kicks requires three-dimensional simulations where a fixed inner boundary is not necessary and the proto–neutron star is allowed to move.

This research has been supported by NASA (NAG5-2843, MIT SC A292701, and NAG5-8128), the NSF (AST-97-31569), the US DOE ASCI Program (W-7405-ENG-48), and the Alexander von Humboldt–Stiftung (FLF-1065004). It is a pleasure to thank Ewald Müller, Thomas Janka, Stan Woosley, Andrew MacFadyen, and Norbert Langer for encouragement and advice.

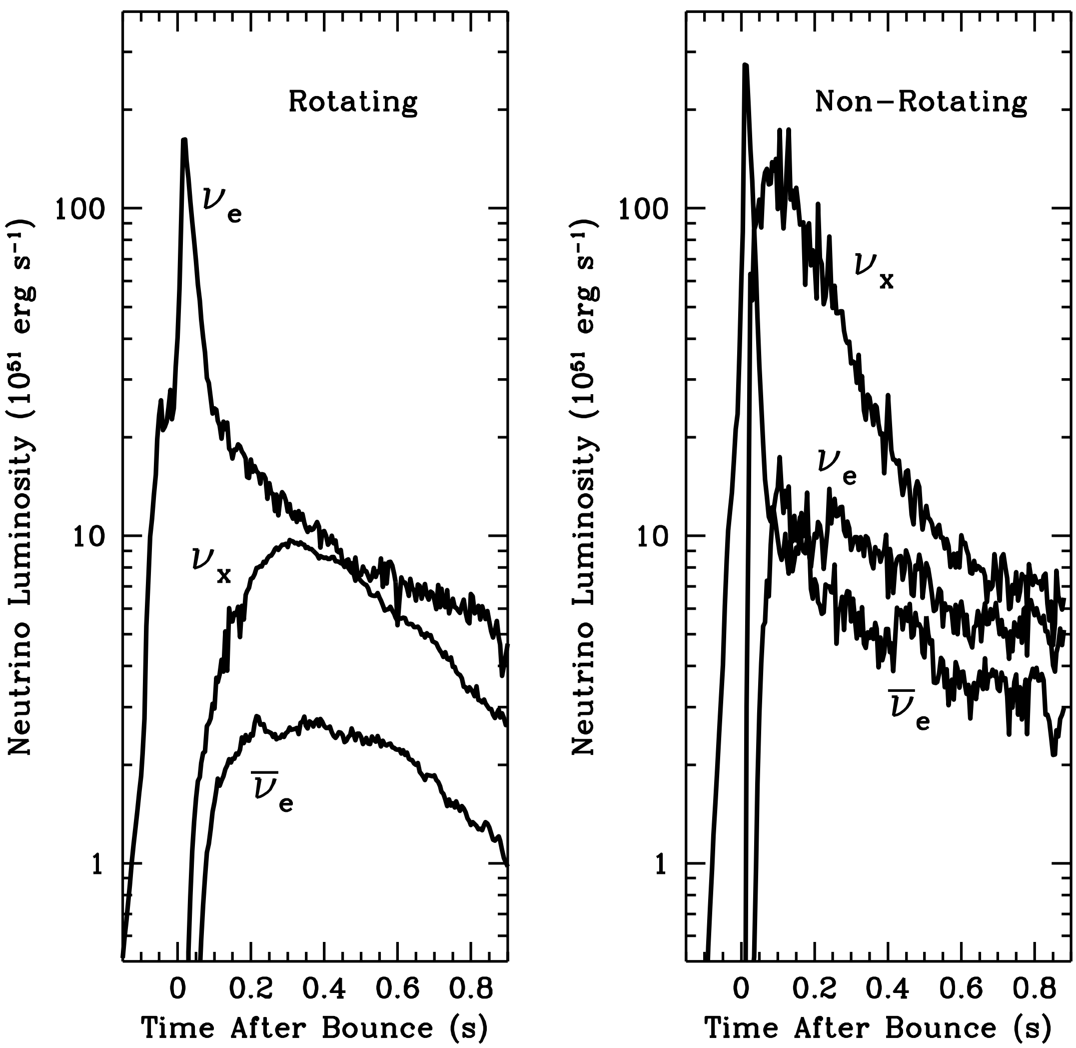

FIG. 15.—Neutrino luminosities vs. time for a rotating and a nonrotating progenitor (models 1 and 6). The nonrotating core has a much larger μ and $\tau(\nu_x)$ neutrino luminosity, especially just after bounce. This is because the nonrotating core compresses more and, at the μ and τ neutrinosphere, the temperature is over a factor of 1.5 higher than that of the rotating core. Because of the large dependence of neutrino emission on temperature (the luminosity from pair annihilation $\propto T^9$), this small change in temperature has large effects on the neutrino luminosity.

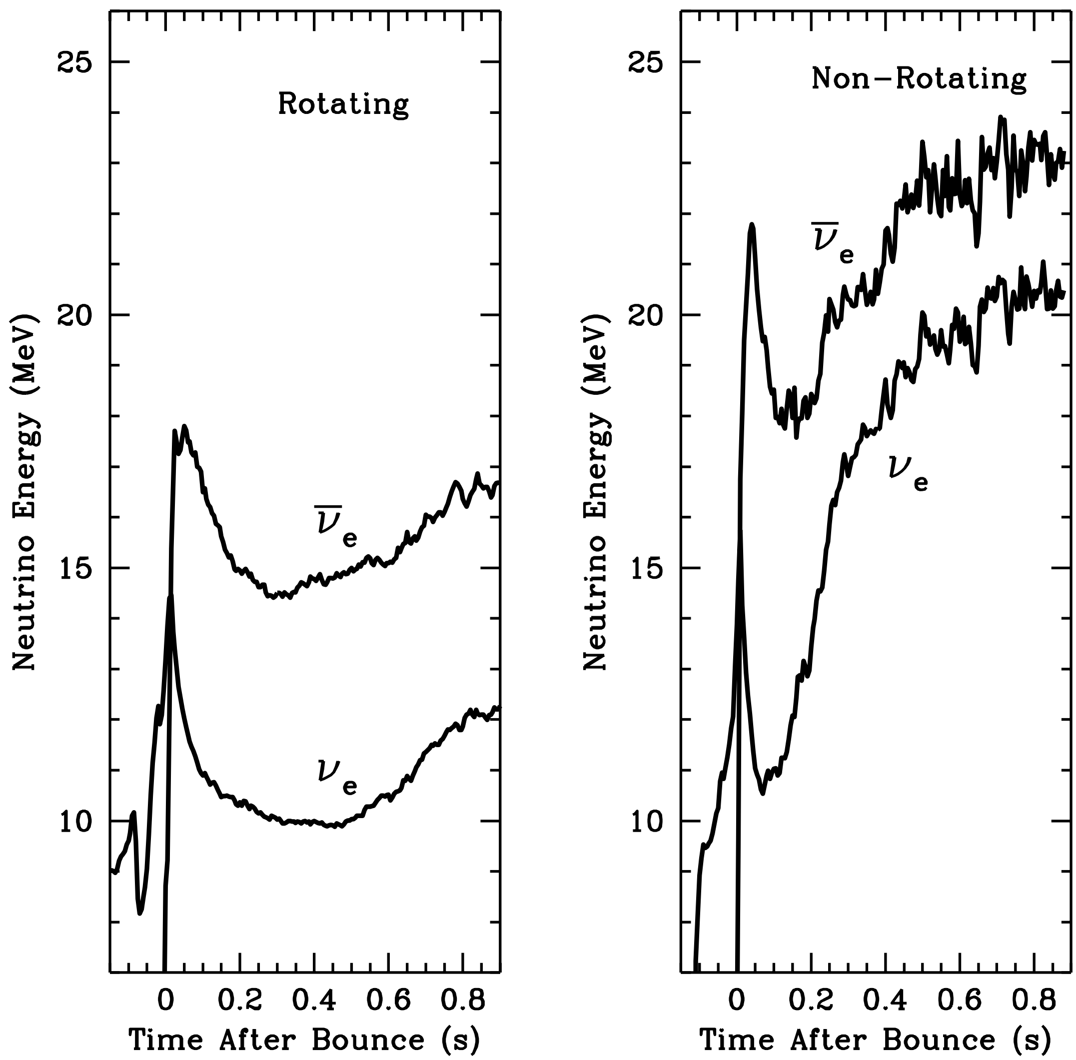

FIG. 16.—Electron and antielectron neutrino energies vs. time for a rotating and a nonrotating progenitor (models 1 and 6). The neutrino energies for the nonrotating core at any given time after bounce are much higher. This is in part due to the larger compression and hence higher temperatures of the nonrotating cores. But most of the difference can be explained by the explosion time. The nonrotating star explodes ~ 0.2 s after bounce, leaving a hot, bare proto–neutron star that continues to cool by emitting neutrinos. The rotating core is still convecting, and its neutrinosphere is farther out where temperatures are lower.

REFERENCES

Blinnikov, S. I., Dunina-Barkovskaya, N. V., & Nadyozhin, D. K. 1996, ApJS, 106, 171
Bodenheimer, P., & Woosley, S. E. 1983, ApJ, 269, 281
Bonazzola, S., & Marck, J. A. 1993, A&A, 267, 623
Burrows, A., & Goshy, J. 1993, ApJ, 416, L75
Burrows, A., Hayes, J., & Fryxell, B. A. 1995, ApJ, 450, 830
Burrows, A., Mazurek, T. J., & Lattimer, J. M. 1981, ApJ, 251, 325
Chaboyer, B., & Zahn, J.-P. 1992, A&A, 253, 173
Colgate, S. A., & White, R. H. 1966, ApJ, 143, 626
Dotani, T., et al. 1987, Nature, 330, 230
Endal, A. S., & Sofia, S. 1978, ApJ, 220, 279
Ergma, E., & van den Heuvel, E. P. J. 1998, A&A, 331, L29
Finn, L. S., & Evans, C. R. 1990, ApJ, 351, 588
Fryer, C. L. 1999, ApJ, 522, 413
Fryer, C. L., Benz, W., Herant, M., & Colgate, S. A. 1999, ApJ, 516, 892
Fryer, C. L., Colgate, S. A., & Pinto, P. A. 1999, ApJ, 511, 885
Fryer, C. L., & Kalogera, V. 1998, ApJ, 489, 244
Fukuda, I. 1982, PASP, 94, 271
Grevesse, N., & Noels, A. 1993, in Origin and Evolution of the Elements, ed. N. Prantzos, E. Vangioni-Flam, & M. Casse (Cambridge: Cambridge Univ. Press), 13
Heger, A. 1998, Ph.D. thesis, Technische Univ. München
Heger, A., Langer, N., & Woosley, S. E. 2000, ApJ, 528, 368
Herant, M., Benz, W., Hix, W. R., Fryer, C. L., & Colgate, S. A. 1994, ApJ, 435, 339
Hix, W. R., & Thielemann, F. K. 1996, ApJ, 460, 869
Höflich, P., Wheeler, J. C., Hines, D., & Trammell, S. 1995, ApJ, 459, 307
Janka, H.-T., & Mönchmeyer, R. 1989, A&A, 209, L5
Janka, H.-T., & Müller, E. 1996, A&A, 306, 167
Janka, H.-T., Zwerger, T., & Mönchmeyer, R. 1993, A&A, 268, 360
Keil, W., Janka, H.-T., & Müller, E. 1996, ApJ, 473, L111
Lattimer, J. M., & Swesty, F. D. 1991, Nucl. Phys. A, 535, 331
LeBlanc, J. M., & Wilson, J. R. 1970, ApJ, 161, 541
Ledoux, P. 1947, ApJ, 105, 305
Lindblom, L., Mendell, G., & Owen, B. J. 1999, Phys. Rev. D, 60, 064006
Lindblom, L., Owen, B. J., & Morsink, S. N. 1998, Phys. Rev. Lett., 80, 4843
Livio, M., & Pringle, J. E. 1998, ApJ, 505, 339
MacFadyen, A., & Woosley, S. E. 1999, ApJ, 524, 262
Marshall, F. E., Gotthelf, E. V., Zhang, W., Middledich, J., & Wang, Q. D. 1998, ApJ, 499, L179
Matz, S. M., et al. 1988, Nature, 331, 416
Messer, O. E. B., Mezzacappa, A., Bruenn, S. W., & Guidry, M. W. 1998, ApJ, 507, 353
Mezzacappa, A., Calder, A. C., Bruenn, S. W., Blondin, J. M., Guidry, M. W., Strayer, M. R., & Umar, A. S. 1998a, ApJ, 493, 848
———. 1998b, ApJ, 495, 911
Miller, D. S., Wilson, J. R., & Mayle, R. W. 1993, ApJ, 415, 278
Mönchmeyer, R., & Müller, E. 1989, in Timing Neutron Stars, ed. H. Ögelman & E. P. J. van den Heuvel (NATO ASI Ser. C, 262; New York: ASI), 549
Mönchmeyer, R., Schäfer, G., Müller, E., & Kates, R. E. 1991, A&A, 246, 417
Müller, E., & Hillebrandt, W. 1981, A&A, 103, 358
Müller, E., Różyczka, M., & Hillebrandt, W. 1980, A&A, 81, 288
Pinsonneault, M. H., Kawaler, S. D., Sophia, S., & Demarque, P. 1989, ApJ, 338, 424
Rampp, M., Müller, E., & Ruffert, M. 1998, A&A, 332, 969
Shakura, N. I., & Sunyaev, R. I. 1973, A&A, 88, 23
Spruit, H. C. 1998, A&A, 333, 603
Spruit, H. C., & Phinney, E. S. 1998, Nature, 393, 193
Spyromilio, J., Meikle, W. P. S., & Allen, D. A. 1990, MNRAS, 242, 669
Sunyaev, R., et al. 1987, Nature, 330, 227
Symbalisty, E. M. 1984, ApJ, 285, 729
Tassoul, J. L. 1978, in Theory of Rotating Stars, ed. J. Ostriker (Princeton: Princeton Univ. Press)
Thompson, C., & Duncan, R. C. 1993, ApJ, 408, 194
Tohline, J. E., Schombert, J. M., & Boss, A. P. 1980, Space Sci. Rev., 27, 555
Trimble, V. 1991, A&A Rev., 3, 1
van Riper, K. A. 1979, ApJ, 232, 558
Wang, L., & Wheeler, J. C. 1998, ApJ, 504, L87
Wang, L., Wheeler, J. C., Li, Z. W., & Clocchiatti, A. 1996, ApJ, 467, 435
Weaver, T. A., Zimmermann, G. B., & Woosley, S. E. 1978, ApJ, 225, 1021
Wilson, J. R., & Mayle, R. W. 1988, Phys. Rep., 163, 63
Woosley, S. E., & Weaver, T. A. 1995, ApJS, 101, 181
Yamada, S., & Sato, K. 1994, ApJ, 434, 268
———. 1995, ApJ, 450, 245
Zahn, J.-P. 1975, Mém. Soc. R. Sci. Liège, 8, 31
———. 1992, A&A, 265, 115
Zwerger, T., & Müller, E. 1997, A&A, 320, 209